DEFECT DETECTION OF GFRP/NOMEX HONEYCOMB SANDWICH STRUCTURE BY LINEAR FREQUENCY MODULATION INFRARED THERMAL IMAGING

by

Qing-Ju TANG**, *Wei-Ming FAN*, *Juan JI*, and *Ya-Fei SONG

[a] School of Mechanical Engineering,
Heilongjiang University of Science and Technology, Harbin, China

Original scientific paper
https://doi.org/10.2298/TSCI2106611T

Honeycomb sandwich material is a new material widely used in many fields, but it is easy to produce defects such as delamination and ponding in the process of manufacturing and service. First, a honeycomb sandwich sample containing delamination defects and water accumulation was built. Then, a linear frequency modulated driving halogen lamp is used as the excitation source. Finally, the surface thermal image sequence of the test sample is acquired by infrared thermal imager. Image sequences are processed by inter-frame difference-multi-frame cumulative average method, principal component analysis, Fourier transform method, and logarithmic polynomial fitting method, respectively. Define and calculate the signal-to-noise ratio of the heat map processed by each algorithm. Compared with the other three algorithms, the principal component analysis method processed the image with the highest signal-to-noise ratio and high contrast. This algorithm achieves effective identification of delamination defects and water accumulation in GFRP/Nomex honeycomb sandwich structure.

Key words: *GFRP/Nomex, linear frequency modulation, signal-to-noise ratio analysis, image sequence processing*

Introduction

Honeycomb sandwich material is one of the important structural forms in the field of composite materials, which has been widely used in spacecraft, ships and other fields because of its advantages such as high specific strength, good impact resistance, vibration damping and microwave permeability [1-3]. Because the honeycomb sandwich structure has more production steps, the process is complex, the service environment is more severe, producing delamination, water accumulation and other defects, therefore, seriously affect the material performance and there are huge safety risks [4]. Therefore, in order to maintain the good performance of GFRP/Nomex honeycomb sandwich structure, it is very necessary to adopt advanced non-destructive testing technology to detect and evaluate the defects of honeycomb sandwich structure efficiently, reliably and accurately.

As an emerging non-destructive testing technology, infrared thermal imaging non-destructive testing technology has the advantages of non-contact, high efficiency, safety and intuition compared with conventional testing technology [5, 6]. Linear frequency modulation thermal imaging inspection technology can detect defects of different depths and types at one

* Corresponding author; e-mail: tangqingju@126.com

time, however, there are relatively few studies on the detection of defects in GFRP/Nomex honeycomb sandwich structures using linear frequency modulation thermal imaging method.

In this paper, linear frequency modulated infrared thermodiagramy was applied to examine the honeycomb sandwich structure samples containing delamination defects and water accumulation defects, and the influence law of geometric characteristics of different types of defective on the surface temperature difference was obtained. Principal component analysis (PCA) was used to process the image sequences acquired by the infrared thermal imager, and it achieved effective identification of delamination defects and water accumulation defects in GFRP/Nomex honeycomb sandwich structure.

Testing principle and test system construction

The linear frequency modulated infrared thermal imaging method is a new method of non-destructive testing that combines infrared thermal imaging technology with linear frequency modulated pulse radar detection technology, which uses thermal signals of different frequencies to excite the sample, effectively making up for the shortcomings of the pulse method and the phase-locked method, and can achieve the detection of defects of different depths and types [7]. The principle is that the heat generated by a halogen lamp causes a temperature difference on the surface of the object under test, and then use infrared thermal imager to collect the surface temperature signal of the stimulated sample and transmit the signal to a computer. Figure 1 is the working principle diagram.

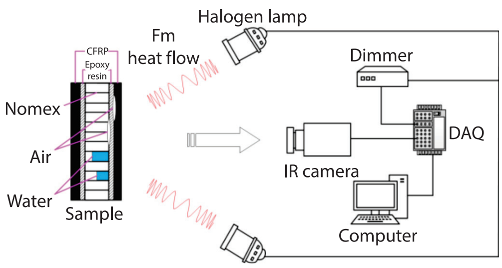

Figure 1. Working principle diagram

The data analysis software is applied to analyze the harvested image sequence signals in time and frequency domains for the purpose of identifying defects.The heat-flow consists of two-components, the static component and the dynamic component [8]. The surface heat-flow $q(t)$ reads:

$$q(t) = q_S + q_D = \frac{q_{max}}{2}\left\{1+\sin\left[2\pi\left(f_0 + \frac{f_e - f_0}{2T}t\right)t\right]\right\},\ t \in [0, T] \tag{1}$$

where q_{max} is the peak surface heat-flow, q_S – the static component of the surface heat-flow, q_D – the surface heat-flow component, f_0 – the initial frequency of the Chirp modulation signal, f_e – the cut-off frequency of the Chirp modulation signal, and T – the scan period of the Chirp modulation signal. It is easy to see that eq. (1) is the linear chirp modulation heat-flow excitation equation.

The test system was built according to the test principle, in which the peak power of a single halogen lamp is 1000 W, the infrared thermal imager model is FLIR A655SC, pixel resolution is 640 × 480, thermal sensitivity is 0.03 °C, and the data acquisition card model is NI-USB6259BNC.

Test

Sample preparation

The GFRP/Nomex honeycomb sandwich structure consists of epoxy resin bonded upper and lower skin and honeycomb core. Table 1 shows the specific processing dimensions of the test piece defects. Among its, the first and second columns use blind holes to simulate delamination defects with different diameters and depths, in the third and fourth columns, needle tube water injection was used to simulate the defects of porous water (2-5 holes) and single-hole water, respectively.

Table 1. Defect machining dimensions of samples

Row \ Column	1	2	3	4
1	*DA* = 6	*DA* = 6	*DA* = 6	*DH* = 0.6
	DL = 0.5	*DL* = 0.6	*DL* = 4.6	*DL* = 0.6
2	*DA* = 8	*DA* = 8	*DA* = 8	*DH* = 1.2
	DL = 0.5	*DL* = 0.6	*DL* = 4.6	*DL* = 0.6
3	*DA* = 10	*DA* = 10	*DA* = 10	*DH* = 1.8
	DL = 0.5	*DL* = 0.6	*DL* = 4.6	*DL* = 0.6
4	*DA* = 12	*DA* = 12	*DA* = 12	*DH* = 2.4
	DL = 0.5	*DL* = 0.6	*DL* = 4.6	*DL* = 0.6

* where DA is defect diameter [mm], DL – the defect depth [mm], and DH – the height of water [mm]

Test parameters

As shown in tab. 2, the halogen lamp power was set to 800 W, chirp initial frequency was 0.1 Hz, chirp termination frequency was 0.05 Hz, and scanning period was 20 seconds to apply heat-flow excitation the sample. The sampling frequency of thermal imager was set to 20 Hz and acquisition time to 40 seconds to complete the image sequence acquisition.

Table 2. Parameters of detection test

Power, P [W]	Original frequency, f_0 [Hz]	Termination frequency, f_ε [Hz]	Scanning time, T [s]	Sampling frequency [Hz]	Sampling time [s]
800	0.1	0.05	20	20	40

Test results and analysis

Applying linear frequency modulated heat-flow excitation thesample, fig. 2 shows the original heat map after normalization at different times.

It can be seen from fig. 2 that after applying linear frequency modulation heat-flow excitation the test piece, the defects on the surface of the test piece have appeared in 5 seconds, at 20 seconds, defects are more obvious than ever. When the sample is heated to 40 seconds, the sample has gradually entered the thermal equilibrium state, and the defect edge is not clear, and the image quality is poor.

Influence of delamination geometric characteristics on surface temperature difference

Figures 3(a) and 3(b) show the influence of different delamination diameters and depth on surface temperature difference, respectively.

Figure 3(a) shows that for defects with the same depth, the larger the delamination diameter is, the more heat accumulated at the defects due to heat insulation, and the larger the temperature difference is, the more easily the defects will be captured by thermal imagers. It

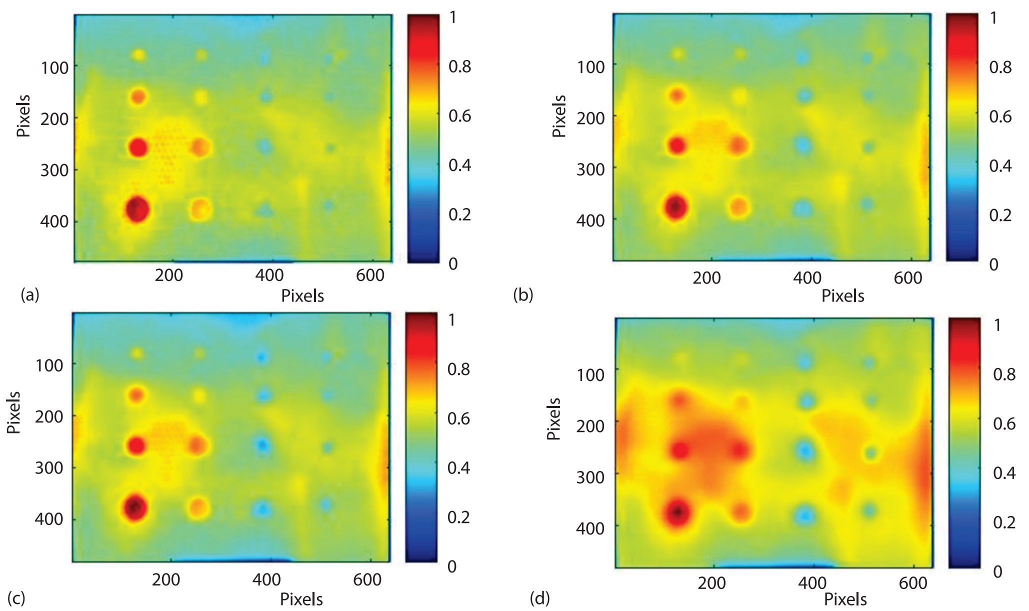

Figure 2. Original heat maps at different times; (a) 5 seconds, (b) 10 seconds, (c) 20 seconds, and (d) 40 seconds

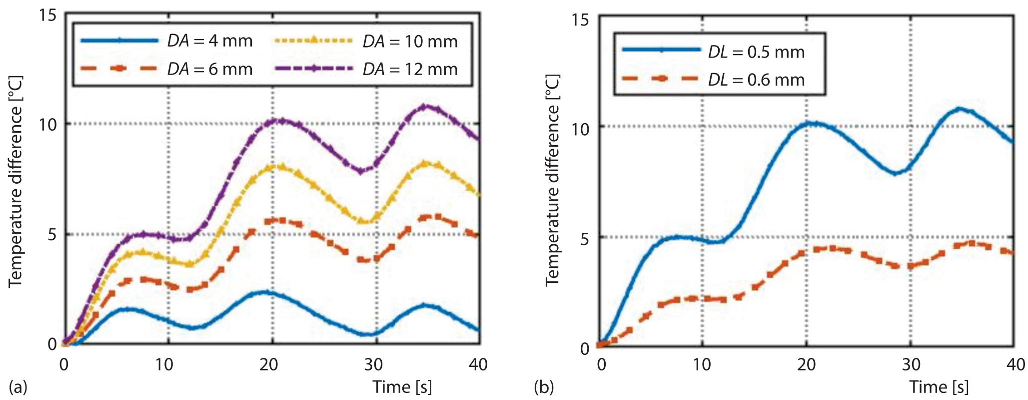

Figure 3. Effect of different delamination defects on surface temperature difference; (a) different diameters and (b) different depths

can be seen from fig. 3(b) that when the defect diameter is the same, the shallower the defect, the greater the surface temperature difference, the easier to detect the defect.

Influence of geometrical characteristics of water accumulation on surface temperature difference

Figures 4(a) and 4(b), respectively show the influence of different single-hole water height and porous water on surface temperature difference.

Figures 4(a) and 4(b) show that the surface temperature of the defective area is smaller than that of the defect free area because the thermal conductivity of the defective area is larger than that of the defect free area. Therefore, the higher the height of water, the greater the temperature difference between defect and non-defect on thesample surface, the easier the defect detection. By analogy, the larger the water area, the easier the defect detection.

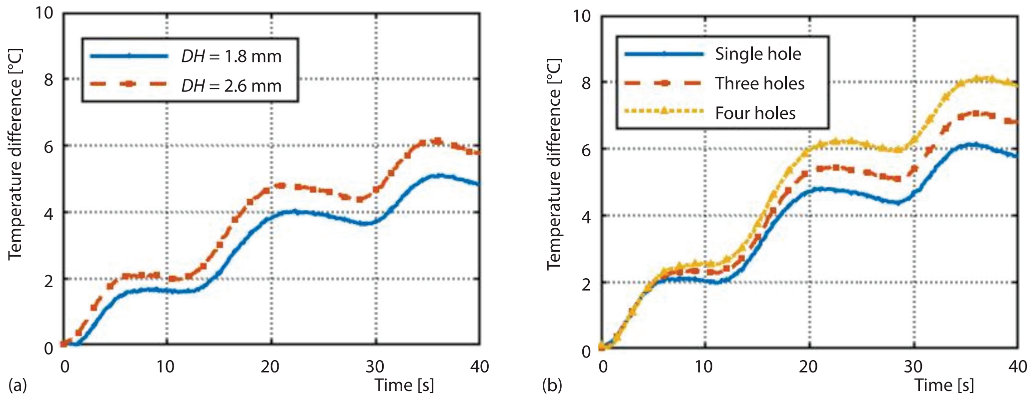

Figure 4. Influence of different water accumulation on surface temperature difference; (a) single hole and (b) multi-hole

Image sequence processing

Inter-frame difference-multi-frame cumulative average method

The advantages of combining the inter-frame difference method with the multi-frame cumulative average method include: this new method can obtain temperature field changes, suppress the influence of static factors, improve the image signal-to-noise ratio (SNR), and eliminate the influence of uneven heating.

Inter-frame difference method

Due to the difference in thermal conductivity between the defective area and the normal area, the accumulation of energy in the defective area results in different temperature changes in the defective area. The difference operation can achieve the effect of highlighting defects. The inter-frame difference method can be divided into forward difference and backward difference. This subject mainly focuses on the image sequence collected during the heating phase, so the backward difference method is used [9]. The first-order backward difference operation of discrete time series is defined:

$$y(n) = \Delta x(n) = x(n) - x(n-1) \tag{2}$$

where $x(n)$ is the signal at time n. It can be seen from eq. (2) that the value of the differential signal at time $x(n)$ is equal to the value at time n minus the value at the previous time (time $n-1$). This value is equal to the rate of change at that moment.

Multi-frame cumulative average method

The multi-frame cumulative average method is a method of adding the corresponding pixel values of two or more frames of images at different times by increasing the integration time, and then calculating the time average to improve the image SNR [10].

An image with noise can be considered as a superposition of target image $f(x, y, t)$, and noise $n(x, y, t)$, and then:

$$g(x, y, t) = f(x, y, t) + n(x, y, t) \tag{3}$$

Time average image obtained by averaging the acquired, M, frame images $\overline{g}(x, y, t)$:

$$\overline{g}(x,y,t)=\frac{1}{M}\sum_{i=1}^{M}g_i(x,y,t) \tag{4}$$

Figure 5 is the result of the original heat map sequence after being processed by the inter-frame difference-multi-frame cumulative averaging method.

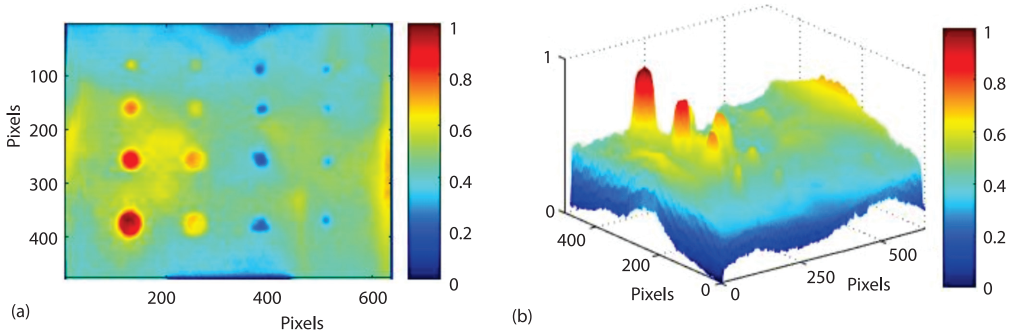

Figure 5. Results of inter-frame difference-multi-frame accumulative average method; (a) 2-D diagram and (b) 3-D diagram

Principal component analysis

The PCA is an effective method to improve the SNR of infrared thermal image sequences. The steps for processing thermal image sequences by this method are [11]:

- Transform the N-frame heat map sequence into $m\times n$-dimensional matrix A. The A_1 has $n_x n_y$ rows (each row is a complete image) and N columns, which become the time component, as shown in fig. 6(a). The A_2 has N rows (each row is a time series) $n_x n_y$ column called spatial component, as shown in fig. 6(b).
- A row vector is extracted from matrix A as the average vector A_{mean}, and all the row vectors in matrix A subtract A_{mean} to eliminate noise effects.
- Calculate $A - A_{\text{mean}}$ covariance matrix or perform singular value decomposition.
- Components are selected from the feature vector to obtain the results.

Figure 7 is the result of the original heat map sequence processed by PCA.

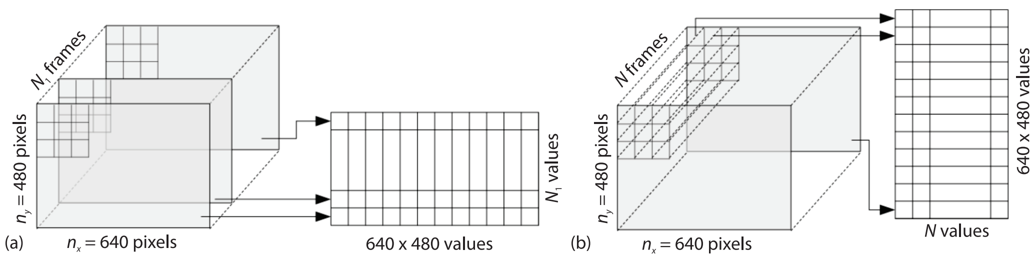

Figure 6. Schematic diagram of PCA; (a) time component A_1 and (b) Spatial component A_2

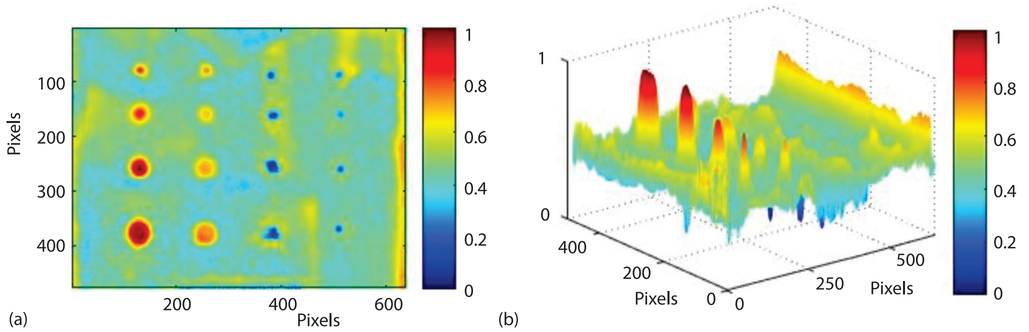

Figure 7. Results of PCA; (a) 2-D diagram and (b) 3-D diagram

Fourier transform method

The discrete Fourier transform is applied to the temperature signals corresponding to each pixel in the thermal image sequence [12]:

$$F_n = \sum_{k=0}^{N-1} T(k)\mathrm{e}^{-j2\pi nk/N} = R_n + jI_n \tag{5}$$

where $T(k)$ is the temperature value of pixel (x, y) in the k frame infrared image, n – the sequence number after frequency dispersion, and R_n and I_n are the real and imaginary parts of the transformed complex numbers, respectively.

According to eq. (5), the amplitude and phase values at frequency n read:

$$A(n) = \sqrt{R_n^{\,2} + I_n^{\,2}} \tag{6}$$

and

$$\phi(n) = \arctan\left(\frac{I_n}{R_n}\right) \tag{7}$$

The amplitude and phase values of all pixels in the infrared thermal image sequence at a given frequency are solved, and the amplitude matrix and phase matrix are composed, respectively, to form the amplitude diagram and phase diagram. The defect recognition is realized by comparing the amplitude and phase diagram. Figure 8 is the result of the original heat map sequence processed by Fourier transform method.

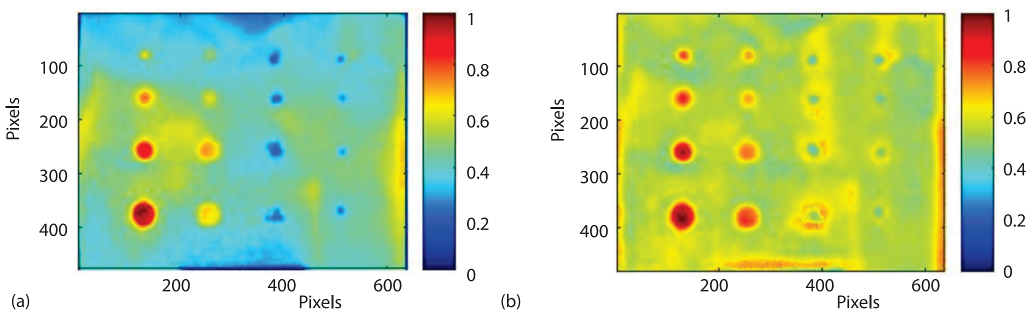

Figure 8. Results of PCA; (a) 2-D amplitude diagram and (b) 2-D phase diagram

Logarithmic polynomial fitting method

The steps of logarithmic polynomial fitting for infrared image are logarithmic processing was performed on the data of each pixel temperature changing with time in the infrared image sequence, and the processed data were fitted by polynomial. The coefficient matrix composed of the same order coefficients of all pixels in the image was extracted, and the coefficient images corresponding to different orders were obtained coefficient matrix to judge the defects of the sample [13]. The polynomial fitting of logarithm of temperature change and time can be given:

$$\ln\left[\Delta T\left(x,y,n\right)\right]=\text{ploynomial}\left[\ln\left(n\Delta t\right)\right] \tag{8}$$

where $\Delta T(x, y, n)$ is the temperature change process of a pixel in the infrared thermal image sequence with time and Δt_n is time change.

Figure 9 is the result graph of coefficient matrix extracted after logarithmic polynomial fitting, a_1, a_2 and a_3 are second-order, first-order and constant term coefficients, respectively.

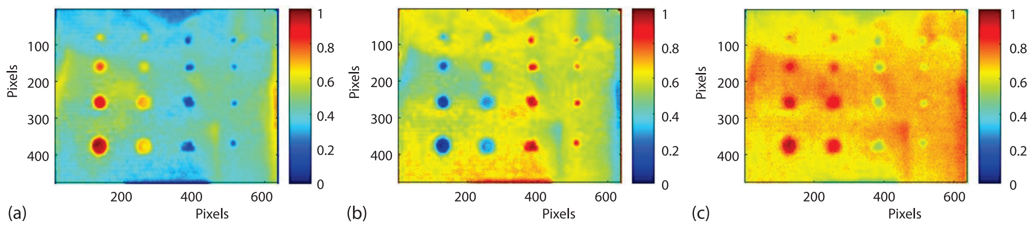

Figure 9. Figures of logarithmic polynomial fitting results; (a) a_1, (b) a_2, and (c) a_3

Algorithm evaluation

In order to evaluate the image processed by the aforementioned four algorithms, the SNR is defined for analysis [14]. The SNR (the SNR is higher, the less the image is affected by noise, and the image quality is higher) reads:

$$SNR=\frac{\left|\overline{P_d}-\overline{P_s}\right|}{\sigma_s} \tag{9}$$

where $\overline{P}_d$, $\overline{P}_s$, and σ_s represent mean eigenvalue of defect area, mean value of eigenvalue of defect free area, and standard deviation of eigenvalue of defect free area, respectively.

The SNR of the images processed by the previous four algorithms is calculated. Figure 10 shows the calculation results of SNR.

By figs. 5, 7-10, the four algorithms suppress the noise and improve the image quality, and the image quality after Fourier transform and PCA is the higher. By calculating the SNR of the image, it can be seen that the SNR of the image processed by PCA is the highest and the image quality is the best.

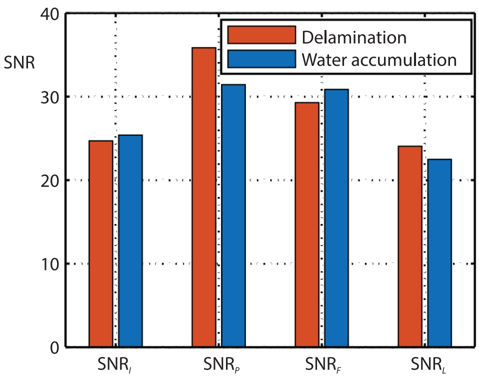

Figure 10. Calculation of SNR

Conclusion

In order to detect the defects of delamination and water accumulation in GFRP/Nomex honeycomb sandwich structure, a linear frequency modulation thermal imaging system was established. Through halogen lamp excitation, the original thermal image sequence is collected by thermal imager. Aiming at the problem of noise interference in heat map sequence, four algorithms such as Fourier transform are used to process the original heat map sequence. According to the calculation, compared with the other three algorithms, the SNR of the image processed by PCA is the highest, and the effective extraction of image surface defect information is realized.

Acknowledgment

This project is supported by National Natural Science Foundation of China (Grant No. 51775175), Heilongjiang Science and Technology Plan Provincial Hospital Science Technology Cooperation Project (Grant No. YS18A18), and Heilongjiang Province Natural Science Fund (Grant No. LH2021E088).

Nomenclature

f – chirp frequency, [Hz]
q – surface heat-flow, [Wm^{-2}]
$\Delta T(x, y, n)$ – pixel value changes over time, [°C]
Δt_n – time change, [s]

Reference

[1] Dou, M. Y., *et al*., Buckling and Post-Buckling of Nomex Honeycomb Cores Under Compression, *Journal of Nanjing University of Aeronautics & Astronautics*, *51* (2019), 1, pp. 69-74
[2] Liu Y., *et al*., A Damage Pattern Recognition Method for Hypervelocity Impact on Aluminum Honey-Comb Core Sandwich Based on Acoustic Emission, *Acta Aeronautica et Astronautica Sinica*, *38* (2017), 5, pp. 220401-220401
[3] Tian, X., *et al*., Preparation and Application of Honeycomb Sandwich Struture Composites, *Shandong Textile & Technology*, *57* (2016), 1, pp. 7-9
[4] Zhang, J. M., *et al*., Research Progress on Preparation Technology and Application of Aramid Paper Honeycomb Core Materials (in Chinese), *Advanced Materials Industry*, (2019), 12, pp. 52-56
[5] Tang, Q. J., *et al*., Experimental Research on ysz tbc Structure Delamination Defect Detection Using Long-Pulsed Excitation of Infrared Thermal Wave Non-Destructive Testing, *Thermal Science*, *23* (2019), 3A, pp. 1313-1321
[6] Tang, Q. J., *et al*., Theoretical Study on Infrared Thermal Wave Imaging Detection of Semiconductor Silicon Wafers with Micro-Crack Defects, *Thermal Science*, *24* (2020), 6B, pp. 4011-4017
[7] Liu, J. Y., *et al*., Infrared Thermal Wave Imaging Detection Technology Ex-Cited by Linear Frequency Modulation, *Infrared and Laser Engineering*, *41* (2012), 06, pp. 1416-1422
[8] Gong, J. L., *et al*., A Study on the SNR Performance Analysis of Laser-Generated Bidirectional Thermal Wave Radar Imaging Inspection for Hybrid C/GFRP Laminate Defects, *Infrared Physics & Technology*, *111* (2020), 7, 103526
[9] Yu, H. M., *et al*., Multi-Moving Target Detection and Segmentation Based on Level Set (in Chinese), *Journal of Zhejiang University*, (2007), 3, pp. 412-417
[10] Li, H. Q., *et al*.,Application of Multi – Frame Accumulation Average Technology in Infrared Real – Time *Image Processing, Laser & Infrared*, (2005), 12, pp. 978-979 + 982
[11] Tang, Q. J., *et al*., Pulse Infrared Thermal Imaging Detection of Internal Defects in Heat Resistant Alloy Coating Structure Plate, *Infrared and Laser Engineering*, *42* (2013), 7, pp. 1685-1690
[12] Feng, Z., *et al*., Research on Image Processing Algorithm of Infrared Non-Destructive Testing, *Infrared*, *30* (2009), 6, pp. 5-10
[13] Liu, Y., *et al*., Pulsed Infrared Thermodiagramy Processing and Defects Edge Detection Using FCA and ACA, *Infrared Physics and Technology*, *72* (2015), 2, pp. 90-94
[14] Tang, Q. J., *et al*., Infrared Microthermal Imaging Detection of Microcrack Defects in Semiconductor Silicon Wafer, *Journal of Heilongjiang University of Science and Technology*, *31* (2021), 2, pp. 177-183

Paper submitted: January 12, 2021
Paper revised: March 11, 2021
Paper accepted: April 26, 2021